Trends in Photochemistry & Photobiology
Vol. 14, 2012

Review

Application of photoacoustic calorimetry in chemistry and biology

Randy W. Larsen*, William A. Maza, Tarah A. Word and Carissa M. Vetromile
Department of Chemistry, University of South Florida, Tampa, FL 33620, USA

ABSTRACT

Photoacoustic calorimetry (PAC) has emerged as an important tool for obtaining thermodynamic information, including enthalpy and molar volume changes, associated with photo-initiated processes for both chemical and biological systems on the nanosecond to microsecond time scale. This technique can provide energetic information, specifically enthalpies, critical to fully understanding reaction mechanisms in chemical and biological reaction mechanisms provided the process can be photo-initiated. In addition to enthalpies, PAC data gives molar volume changes accompanying the enthalpy changes. Changes in molar volume can provide key insights into the relationship between solvent and reaction intermediates. Here, the theory behind PAC is presented as well as several examples of applications of PAC to biological and chemical systems.

KEYWORDS: photoacoustic calorimetry, time-resolved calorimetry, ligand migration in heme proteins, myoglobin, microperoxidase-11, photoinduced spin crossover, spin cross-over complex, salten mepepy, reverse micelle, Ru(II)[tris-(2,2'-bipyridine)], methyl viologen, electron transfer

1. INTRODUCTION

Understanding reaction mechanisms in both chemical and biological systems requires a detailed understanding of both the structural changes (including bond cleavage/formation processes and conformational changes) as well as the energetics that drive these structural changes. Structural changes associated with reactions can be obtained either through x-ray crystallography or NMR spectroscopy for the reactant molecules, product molecules and any intermediates that can be 'trapped' during the reaction. Alternatively, time resolved optical and vibrational methods can be utilized to characterize reaction intermediates that may exist transiently on time scales ranging from femtoseconds to milliseconds.

Obtaining the thermodynamics associated with reaction intermediates is more challenging. Equilibrium thermodynamic parameters can be easily obtained using the relationship between the Gibbs free energy and the equilibrium binding constant for various ligands (the van't Hoff equation) [1]:

$$\frac{dln(K_{obs})}{d(1/T)} = -\frac{\Delta H^{\circ}}{R} \quad (1)$$

where K_{obs} is the ligand association constant, T is the temperature, R is the gas constant and ΔH^{o} is the reaction enthalpy. Alternatively, reaction enthalpies are determined by obtaining reaction rate constants (Fig. 1) as a function of temperature using the Eyring equation [2]:

$$ln\left(\frac{k_{obs}h}{k_bT}\right) = \frac{\Delta S^{\neq}}{R} - \frac{\Delta H^{\neq}}{RT} \quad (2)$$

where k_{obs} is the observed rate, h is Plank's constant, k_b is Boltzmann's constant and T is the

*Corresponding author
rwlarsen@usf.edu

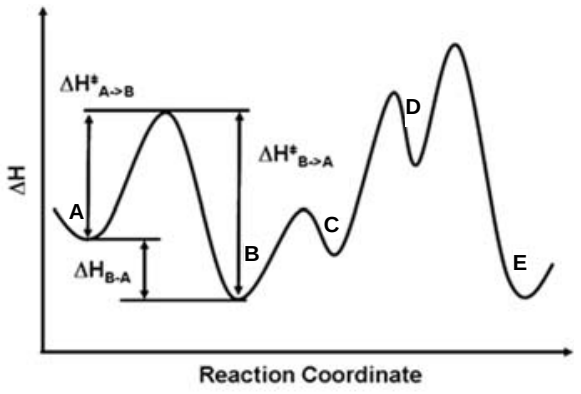

Fig. 1. Schematic diagram illustrating a reaction enthalpy profile including activation parameters.

temperature. However, this strategy presumes the rate constants for both the forward and reverse reactions can be obtained. This is often not the case for reactions which have large forward rate constants and small reverse rate constants or for photo-initiated processes in which the initial photo-product occurs within the initiating light pulse.

Changes in molar volume during the course of a reaction can also provide important mechanistic details with regard to changes in bond lengths, bond cleavage/formation and the role of the solvent in stabilizing reaction intermediates. Equilibrium volume changes can be determined by obtaining the equilibrium constants as a function of pressure according to [3]:

$$\frac{dln(K_{obs})}{dP} = -\frac{\Delta V^{\circ}}{RT} \tag{3}$$

where P is the pressure. The change in molar volume between intermediates can also be determined by obtaining the rate constants as a function of pressure according to:

$$\frac{dln(k_{obs})}{dP} = -\frac{\Delta V^{\neq}}{RT} \tag{4}$$

where P is the applied pressure [3]. However, as with the enthalpy changes described above, the molar volume can only be determined for reaction intermediates with discernible forward and back rate constants.

An alternative to these traditional methods for obtaining reaction thermodynamics are the photothermal methods including photoacoustic calorimetry, thermal lensing, photothermal deflection and transient grating techniques. These methods measure heat and molar volume changes directly on time scales ranging from picoseconds to tens of milliseconds and provide an excellent complement to optical spectroscopies for probing the mechanisms of photo-triggered reactions in chemistry and biology.

2. Photoacoustic calorimetry: Theory and practice

Photoacoustic calorimetry (PAC) has been employed to investigate the magnitudes and lifetimes of enthalpy and molar volume changes associated with many chemical biological systems, including, ligand binding, protein folding/unfolding, electron transfer, photo-initiated spin cross-over, excited state processes in transition metal complexes and signal transduction, to name only a few [4-12]. The PAC signal originates from photoexcitation of a molecule in solution which results in a transition from its ground state (S_0) to a higher excited electronic state (S_n) following Fermi's Golden Rule (Fig. 2). Deactivation of this state may occur through emission of a photon (fluorescence), non-radiative relaxation, and intersystem crossing (triplet state formation). Photoexcitation may also initiate chemical processes including bond breakage/ formation, electron transfer etc. as well as change in molecular conformation (e.g. *cis-trans* isomerization) and intermolecular charge redistribution (e.g. change in dipole) resulting in change in solvent density. If the sample in question undergoes a photo-chemical transformation in addition to the non-radiative decay then excitation of the sample induces rapid density changes due to both thermal heating to the surrounding solvent and solvent-molecule interactions. In aqueous solutions this rapid heating is described by [13-15]:

$$T(r,t) = \frac{2\alpha E_a}{\pi\rho C_p \hbar\omega} \tag{5}$$

where α is the absorption coefficient, E_a is the total energy per pulse, ρ is the density of the solvent, and C_p is the specific heat capacity of the solvent. This change in temperature results in a density change which gives rise to both a pressure wave and a change in refractive index.

PAC utilizes the fact that this rapid change in temperature induces a change in volume of

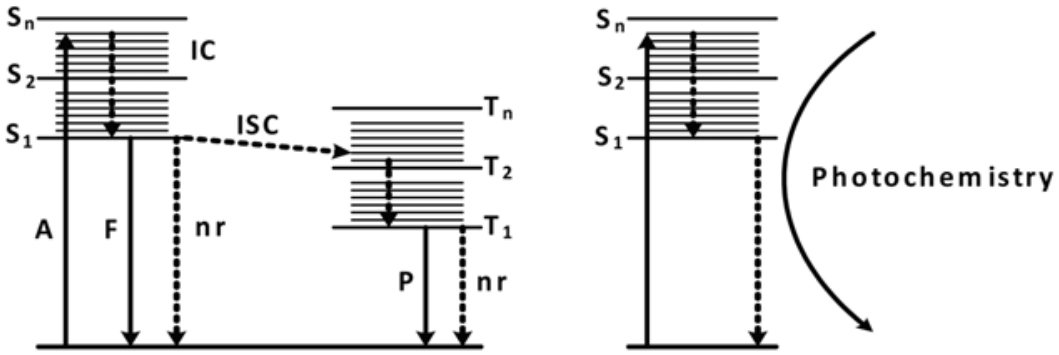

Fig. 2. (left) Perrin-Jablonski diagram describing activation and deactivation of excited states and (right) events observed with photothermal methods after excitation.

the illuminated solution that is proportional to the thermal expansion coefficient of the solvent [15, 16]:

$$\Delta V = \beta \Delta T \tag{6}$$

This volume change generates a change in pressure by [14]:

$$\Delta P = -\left(\frac{1}{\kappa_T}\right)\left(\frac{\Delta V}{V}\right)_T \tag{7}$$

where κ_T is the isothermal compressibility of the solvent and ΔV is the volume of the illuminated sample. This newly generated pressure wave gives rise to an acoustic signal that is measured by a piezoelectric transducer.

The measured acoustic signal is directly proportional to the heat deposited and/or molar volume changes of the sample upon photoexcitation [16, 17]. The corresponding PAC signal for the sample can then be expressed as [4, 13, 15, 16, 18, 19]:

$$S_s = KE_a\left[\left(\frac{\beta}{C_p\rho}\right)Q + \Delta V_{con}\right] \tag{8}$$

where K corresponds to the instrument response parameter, β is the coefficient of thermal expansion of the solvent (K^{-1}), ρ is the solvent density (g mL^{-1}), C_p is the solvent heat capacity (cal g^{-1} K^{-1}), Q is the heat released to the surrounding solvent (kcal mol^{-1}), and E_a is the number of Einsteins adsorbed. The change in volume due to all non-thermal relaxations (i.e. conformational changes, chemical processes, electrostatics, etc.) is ΔV_{con}(mL mol^{-1}). The instrument response parameter is unique to each experiment. Thus to eliminate, K, a reference compound is utilized in which the electronic excited state decays through non-radiative relaxation with a quantum yield of unity. In this case, $\Delta V_{con} = 0$ and the energy returned to the solvent Q, is simply $E_{h\nu}$ (by conservation of energy). The resulting acoustic signal can be described by:

$$S_r = KE_a\left(\frac{\beta}{C_p\rho}\right)Q = KE_a\left(\frac{\beta}{C_p\rho}\right)E_{h\nu} \tag{9}$$

where $E_{h\nu}$ is the photon energy of the excitation wavelength. The corresponding ratio of the sample and reference signals then gives:

$$\left(\frac{S_s}{S_r}\right)E_{h\nu} = \phi E_{h\nu} = Q + \left(\frac{C_p\rho}{\beta}\right)\Delta V_{con} \tag{10}$$

in which, Q and ΔV_{con} can be obtained from a plot of $(S_s/S_r)E_{h\nu}$ versus $\rho C_p/\beta$. Since, for aqueous solutions, $\rho C_p/\beta$ is temperature dependent, the Q and ΔV_{con} values can be determined by obtaining acoustic signals for reference and sample as a function of temperature and plotting the amplitude ratios as a function of $C_p\rho/\beta$.

For kinetic processes taking place between the instrument response time scale (i.e., < ~50 ns) and the long time response of the acoustic detector (dependent upon the transducer relaxation time and frequency, typically 20-25 μs) the sample waveform appears frequency shifted relative to the reference wave (Fig. 3). This is due to the fact that the observed acoustic signals are a convolution of the instrument response function (an under-damped oscillator) and exponential heat decay functions. In order to extract the amplitudes and lifetimes of each decay component, the sample

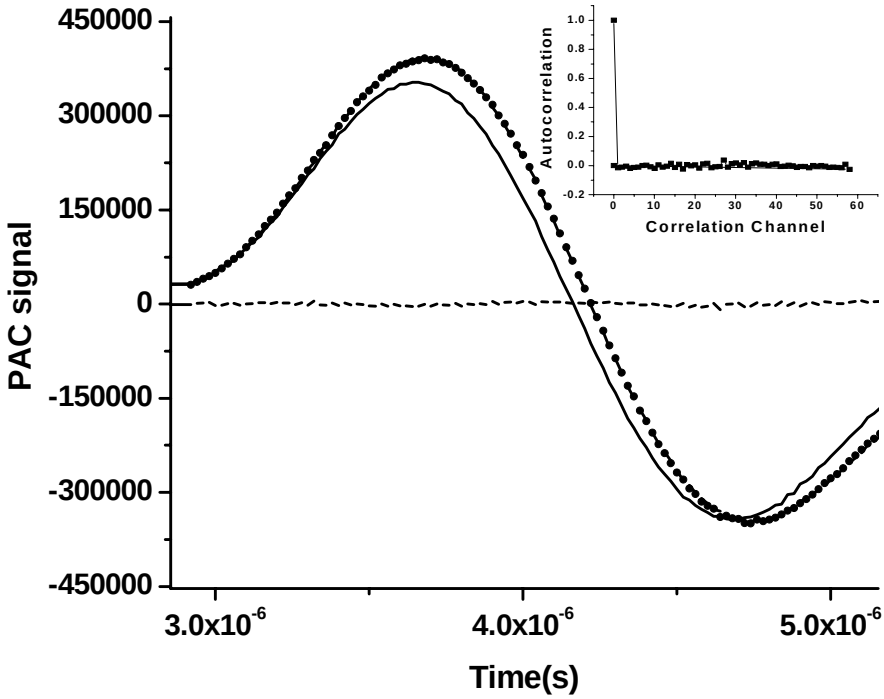

Fig. 3. Overlay of a reference and sample photo-acoustic signal together with a deconvoluted fit to demonstrate time resolution in PAC.

acoustic signal is treated as a convolution between a transducer response function R(t), which in practice is the calorimetric reference, and a heat decay function, H(t), such that:

$$S(t) = R(t) \times \sum_i H_i(t) \tag{11}$$

and:

$$H_i(t) = \left(\frac{\phi_i}{\tau_i}\right) exp\left(-{}^{t}/_{\tau_i}\right) \tag{12}$$

where ϕ_i is the sample acoustic amplitude and τ_i is the lifetime for the i^{th} decay process [13, 18, 19] (Fig. 3). From the heat released (Q_i) the corresponding enthalpy change for each step can be determined:

$$Q_i = -\Phi_i \Delta H_i \tag{13}$$

For the prompt phase Q is subtracted from $E_{h\nu}$ and divided by the quantum yield to obtain ΔH for the process:

$$\Delta H_p = \frac{(E_{h\nu} - Q)}{\Phi} \tag{14}$$

The instrumental set up for PAC (Fig. 4) involves a Quantum Northwest temperature controlled (to within 0.1ºC) 1 cm cuvette sample holder mounted with a Panametrics 20 MHz V103 transducer. The detector is coupled to the cuvette by a thin layer of vacuum grease. Photoexcitation of the sample is generated by a 532nm pulse from a Continuum Minilite I frequency doubled/tripled Q-switched Nd:YAG laser (5-7ns pulse, < 80μJ). Acoustic signals are amplified with an ultrasonic preamp then recorded using a Picoscope 3000 oscilloscope.

3. Photoacoustic studies of ligand photo-release

One class of proteins which have been extensively investigated with respect to the energetics associated with conformational changes arising from ligand binding and catalysis are the heme proteins. Heme proteins are one of the most widely distributed metalloprotein in nature and participate in a plethora of critical physiological processes including electron transfer (cytochromes), mono-oxygenation, peroxide degradation (peroxidases, catalases), sensing (FixL, PAS domain sensors, and HemAT sensors), transcription regulation (CooA type proteins), energy transduction (heme/copper oxidases, cytochrome bc_1, etc.), oxygen transport

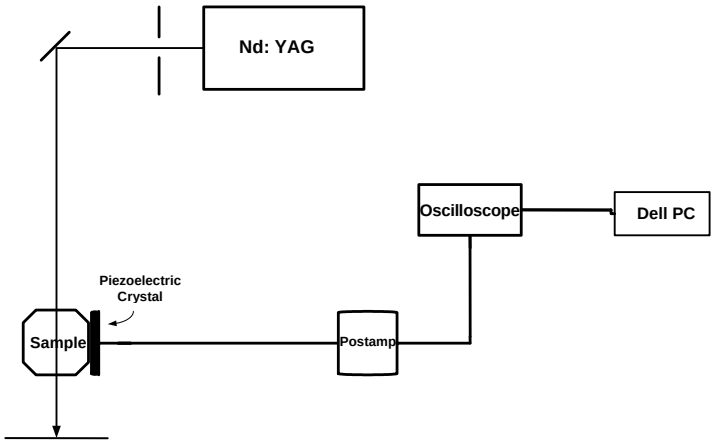

Fig. 4. Schematic diagram of the instrumentation used in photo-acoustic calorimetry.

and storage (hemoglobins and myoglobins) and polymer synthesis/degradation (lignan peroxidase, etc.) [20-22]. The active site in heme proteins is an iron porphyrinic chromophore that is coordinated to the protein through a protein donated ligand (histidine, methionine, tyrosine or cysteine). The catalytic versatility of the heme active site arises from the structural details of the protein matrix. For example, the electronic properties associated with proximal heme ligation can influence the degree of electron back donation into π-accepting ligands in the six-coordination site. Residues constituting the distal heme pocket regulate the orientation of bound ligands in the sixth coordination site as well as the catalytic lability of ligands (such as dioxygen) through H-bond interactions, hydrophobicity, etc. Distal heme pocket residues also make up the substrate binding sites and are designed to place the substrate in a specific orientation and distance from the heme active site in order to facilitate stereo-specific chemistry. Likewise, the protein tertiary structure provides appropriate access channels to and from the heme active site for the substrate which are conformationally regulated. These ligand channels provide ready access from the solvent to the distal heme pocket and can be altered by conformational changes resulting in 'gated' ligand access.

3.1. Heme ligand photolysis

The photo-lability of diatomic ligands such as NO, CO, and O_2 bound to heme iron has provided a dynamic probe for the kinetics of important physiological processes in heme proteins on time scales ranging from femto- to millisecond [5, 23-25]. Photolytic ligand binding studies have revealed a complex interplay between protein structural dynamics, distal heme pocket residues and ligand binding affinity.

3.2. MP11 as a model system

In order to better understand the thermodynamic role of the protein matrix in modulating ligand access to and from the heme active site in heme proteins and enzymes it is necessary to identify the corresponding thermodynamics associated with ligand photo-release from the isolated heme group. This requires an appropriate model system containing an FePPIX as well as a covalently attached proximal base.

Microperoxidase-11 (MP11) is a tryptic digest of Cytochrome C, containing an eleven amino-acid peptide chain covalently attached to a heme group via thioether linkages between two cystine residues (Cys17 and Cys14) and a proximal ligand (His18) providing a high-spin 5-coordinate heme protein model complex (Fig. 5). The 5-coordinate MP11 complex can bind a number of small ligands including O_2 and CO (ferrous MP11), as well as NO and CN^-(ferric MP11). Like heme proteins, the carboxymicroperoxidase-11 (COMP11) complex is photolabile with a high quantum yield. Photolysis of the COMP11 produces a transient five coordinate complex that rebinds CO with pseudo-first order kinetics.

The photolability of the COMP11 complex allows for the characterization of the thermodynamics

associated with CO photo-release using photothermal methods. As the photo-release occurs within the excitation pulse and the subsequent recombination occurs on the time scale of tens of microseconds PAC provides the most appropriate thermodynamic probe. To identify factors contributing to the observed enthalpy and volume changes subsequent to COMP11 photolysis PAC experiments have been performed as a function of solution pH as well as in the presence of surfactants. Here, PAC results for COMP11 photolysis in 50 mM sodium bicarbonate buffer (pH ~12.8 ± 0.1), 50 mMTris buffer (pH ~7.5 ± 0.05), and 0.74 mM sodium dodecyl sulfate, SDS, (pH ~ 7.5 ± 0.05) are summarized. Each sample was dearated with argon gas (~ 5 minutes) and reduced with sodium dithionite to convert the Fe(III)MP11 to Fe(II)MP11.

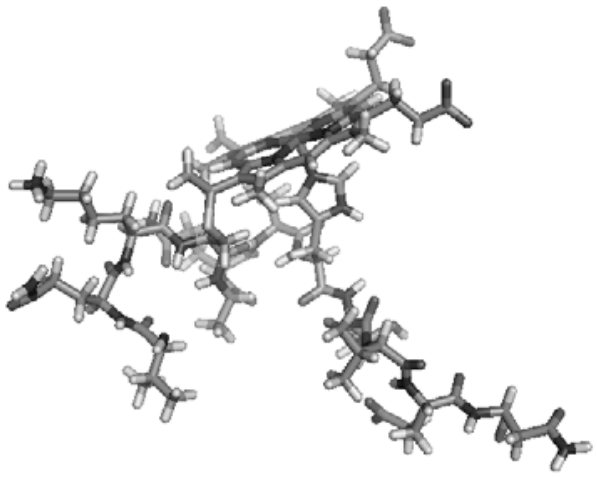

Fig. 5. Structural model of microperoxidase-11 (MP11).

The COMP11 complex is formed by flushing the Fe(II)MP11 with CO to give a final pressure of 1 atm (1 mM solution concentration). A representative PAC trace for the photolysis of COMP11 in 50 mMTris buffer containing 0.74 mM SDS at pH 7.5 together with that of a calorimetric reference compound is displayed in Fig. 6. The absence of a frequency shift between the sample and the reference trace for all samples examined indicates no additional kinetics occurs between ~20 ns and ~20 μs. Plots of ϕE_{hv} versus $C_p\rho/\beta$ gives the molar volume and enthalpy changes associated with COMP11 photolysis and these are summarized in Table I.

In Tris buffer solution pH ~ 7.5, the photolysis of COMP11 is endothermic with a ΔH of 13 kcal mol^{-1} and a ΔV of 11 mL mol^{-1}. Photolysis of the COMP11 complex results in the cleavage of the Fe-CO bond, low- to high-spin transition of the Fe(II) and solvation of the CO. Since the CO is exposed to the solvent the $\Delta V/\Delta H$ contributions arising from solvation are expected to be small. The most significant contributions to ΔH are from the Fe-CO bond energy (~17 kcal mol^{-1}) and to ΔV is the spin state change (~ 10-15 mL mol^{-1}). In fact, the results obtained for CO photolysis from COMP11 are very similar to those obtained subsequent to the photolysis of CO-Fe(II)porphyrin complexes in buffered aqueous solution. In contrast, photolysis of COMP11 in pH ~7.5 in the presence of the anionic surfactant, SDS, or high pH (~12.8) is found to be exothermic (-8 kcal mol^{-1} and -17 kcal mol^{-1}, respectively) and accompanied by a relatively small volume change (~2 mL mol^{-1}).

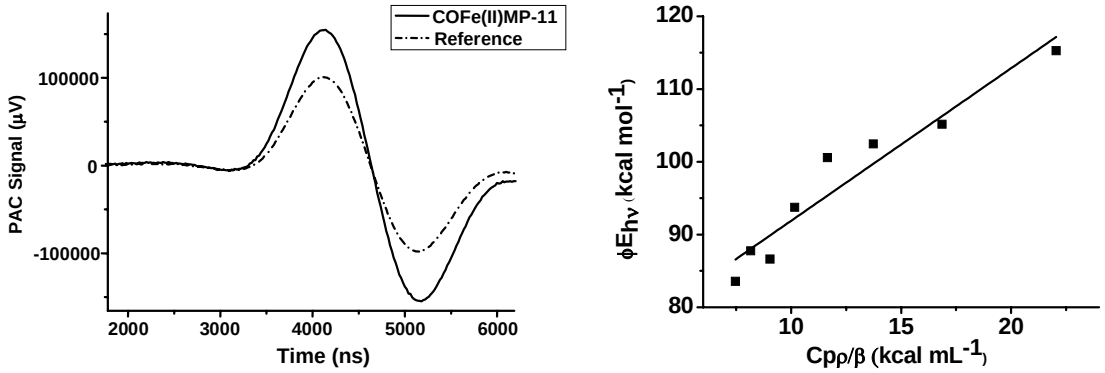

Fig. 6. Typical photoacoustic traces for CO photodissociation of $(CO)Fe^{II}MP11$ vs. Reference (left), in 0.74 mM SDS (pH 7.5) and a plot of S/R^*E_{hv} vs. $C_p\rho/\beta$ (right).

Photolysis of the COMP11 under these solution conditions also results in Fe-CO bond cleavage as well as the spin state change to form the 5-coordinate high-spin complex within the excitation pulse. Subtracting the ΔV and ΔH obtained for the photolysis of COMP11 in aqueous buffered solution from those obtained under high pH conditions or in the presence of SDS indicates additional processes taking place within the excitation pulse but subsequent to the photo-release of CO. The ΔH and ΔV for these processes are found to be -30 kcal mol^{-1} and -9 mL mol^{-1}, respectively, for COMP11 photolysis at pH 7.5 with 0.74 mM SDS ($\Delta H = \Delta H_{obs} - \Delta H_{pH\ 7.5}$, $\Delta V = \Delta V_{obs} - \Delta V_{pH\ 7.5}$) and -21 kcal $mol^{-1}$and -9 mL mol^{-1} for COMP11 at pH 12.8. The molecular origin of the additional processes taking place at high pH or in the presence of SDS is not clear. It has been shown that weak field ligands can destabilize the Fe-His bond in synthetic heme peptides with a resulting loss in peptide secondary structure [26]. For example, the binding of CN^- or N_3^- to the ferric heme peptide analog is accompanied by a ΔH of -19 kcal mol^{-1} and loss of helical character of the covalently attached peptide [26]. However, this was not observed in Fe(III)MP8 [27]. In the case of the Fe(II)MP11 it is possible that at high pH the peptide secondary structure (α helix) is sufficiently destabilized allowing for His dissociation and peptide unfolding in the presence of the anion OH^-.

Alternatively, the ΔH value under high pH conditions would be consistent with a hydroxide molecule binding to the heme iron subsequent to CO photolysis (Fig. 7). Theoretical studies have

Table I. Volume and Enthalpy changes associated with CO photo-release from COMP11 at 532-nm excitation.

	ΔH (kcal mol^{-1})	ΔV (mL mol^{-1})
CO MP11, pH 7.5*	13 ± 3	11.2 ± 0.9
COMP11, pH 12.8	-8 ± 3	2.6 ± 0.6
COMP11, pH 7.5 + 0.74 mM SDS	-17 ± 1	2.1 ± 0.2

*Values reported from Ref. [5]

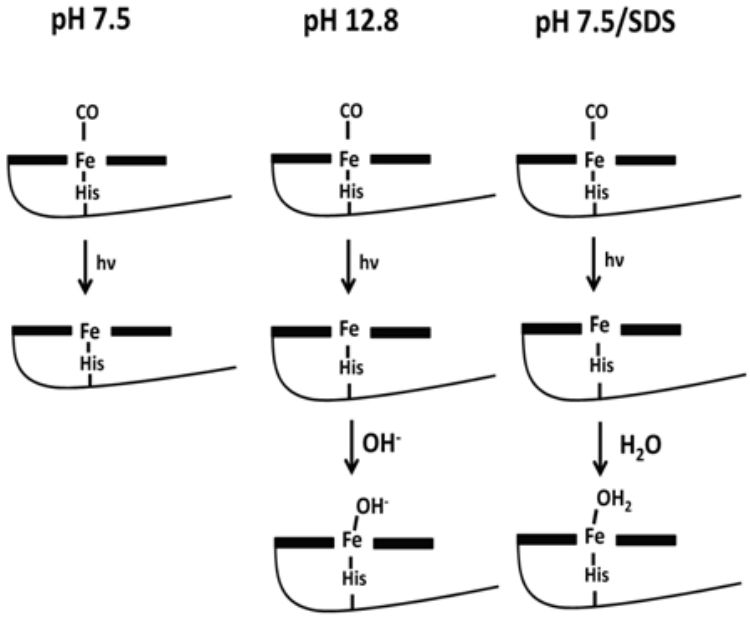

Fig. 7. Schematic diagram, based upon PAC results, illustrating the binding of distal ligands to Fe(II)MP11 subsequent to CO photolysis under varying solution conditions.

demonstrated that the bond dissociation energy of a water molecule to ferrous heme is ~ -30 kcal mol^{-1} versus a ΔH of -21 ± 3 kcal mol^{-1} for the MP-11 [28]. The volume change would also be consistent with a water molecule/hydroxide ion binding. The partial molar volume of water is 18 mL mol^{-1} and that of a hydroxide ion is ~ 21 mL mol^{-1} in aqueous solution [29]. Considering that the OH^- ion is only partially de-solvated upon binding to the ferrous heme iron a molar volume change would be expected to be slightly smaller than that of the isolated OH^- ion.

The origin of the volume and enthalpy changes associated with COMP11 photolysis at neutral pH in the presence of 0.74 mM SDS is less clear. The concentration of SDS is below the critical micelle concentration (2 mM) which precludes effects of micelle encapsulation. However, at neutral pH the two lysine groups associated with MP11 are protonated allowing electrostatic association between the negatively charged SDS head group. Such association could lead to a clustering of surfactant molecules near the heme iron. If surfactant clustering entraps water molecules near the heme active site, photolysis of the COMP11 complex could result in the binding of a water molecule to the heme active site.

4. Photoacoustic studies of ligand migration in heme proteins

Horse heart myoglobin (hhMb) has been extensively utilized as a model heme protein system to better understand the structure-function relationship of small molecule binding [30-38]. The myoglobin three dimensional structure was the first available at high enough resolution to give a complete set of atomic coordinates, unveiling the three-over-three α-helical globin fold. Myoglobin is an oxygen storage heme protein consisting of an iron protoporphrin IX active site coordinated to the protein through a proximal histidine residue located deep within a hydrophobic pocket (Fig. 8) [30-38]. To date, many experimental investigations as well as extensive computational studies have provided a strong foundation for protein dynamics of ligand migration in myoglobin [39, 40]. Still, a clear thermodynamic understanding of the O_2 migration pathway from the heme iron to the solvent, and likewise from the solvent to the heme iron is lacking.

Upon excitation the heme iron back donates electron density to anti-bonding orbitals of gaseous ligands thereby initiating ligand migration [41]. Carbon monoxide, though non-physiological for myoglobin, is often experimentally preferred over other gaseous ligands including O_2 or NO. The photodissociation of CO has an energetic barrier resulting in low geminate rebinding and thus a high quantum yield (near unity) of photocleavage from the ferrous heme. Experimental techniques including optical and vibrational spectroscopies, electrochemical methods, differential scanning calorimetry, etc have provided key insights on the conformational dynamics of CO migration under dilute conditions

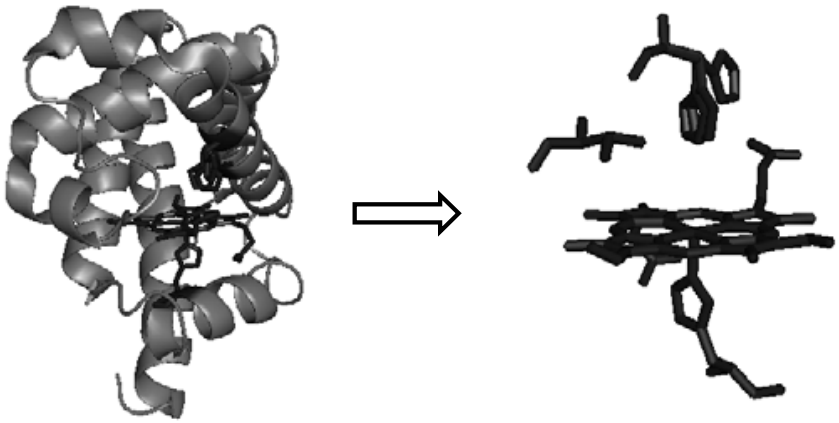

Fig. 8. Ribbon structure of myoglobin (PBD entry 1A6G) and key residues Val67, His63 and His92 of the heme pocket.

or solution conditions. The overall accepted mechanism for physiological temperatures developed from these experiments as well as X-ray crystallography begins with CO bound and the protein structure in a closed conformation with His64 rotated in the protein pocket forming a hydrogen bond network with H_2O - Lys45 - 6-propionate group of the heme (no obvious channel for ligand exit) [42]. Within picoseconds of CO photorelease the ligand migrates to a nearby distal site. The ligand remains near the distal side of the heme for 100-300ns until it traverses to the Xe(1) binding pocket. There is still some disagreement with the final escape to the solvent, however at physiological temperatures it appears that CO exits through a His 'gated' channel with a lifetime of ~800ns for hhMb. The His64 -H_2O - Lys45 - 6-propionate group of the heme H-bond network is disrupted by rotation of His64 out of the distal pocket to form a migration pathway open to the bulk solvent. In addition, X-ray crystallographic data displays a water molecule bound to His64 (~84% occupancy) indicating the entry of a water molecule following CO exit. This water molecule is believed to govern CO entry to the protein matrix. A sequential two barrier model has previously been proposed for CO rebinding kinetics. The outer barrier is characterized by CO entry and the inner barrier assigned to ligand binding to the heme. Specific heat measurements by Kleinert *et al.* concluded that the outer barrier is dependent of viscosity while the inner kinetic barrier is not [37]. In addition, it is believed that the inner barrier ultimately controls rebinding kinetics to the heme binding site.

The general use of CO for elucidating ligand migration in myoglobin has also been employed in numerous theoretical studies [40]. Recently, a theoretical study by Ruscio *et al.* examined CO migration exit and entry to the protein matrix at room temperature [40]. The MD simulations revealed two distinct dynamic pathways for CO migration to the solvent. Multiple trajectory simulations displayed that CO migrates more frequently down one path (major) than the other (minor). Trajectory simulations of CO re-entry also displayed preference down the major pathway [40]. For both exit and entry ligand migration down the major pathway was accompanied with short lived ligand docking involving the Xe(4) and Xe(1) cavities of myoglobin. These results are in good agreement with previous time-resolved experiments, including time-resolved X-ray studies of CO photodissociation from ferrous myoglobin. Ruscio, *et al.* also suggested multiple residues that could also serve as exit portals for CO, however exit through the His portal was observed most often. While these results are consistent with experimental results, according to this work other exit portals to the solvent are possible. Previous photothermal methods have shown that flash photolysis of Mb-CO in pH8 buffered solution conditions results in formation of two fast intermediates (τ<50ns, and τ = 80ns) [32-34]. Angeloni and Feis reported that within the prompt phase (<50ns), photocleavage of CO forms a fast intermediate deoxymyoglobin with CO docked near proximal heme pocket, resulting in a volume contraction of -3mL mol^{-1} and a positive enthalpy change of ~14 kcal mol^{-1} nearly that of the enthalpy change for CO-Fe bond dissociation (17kcal mol^{-1}) [32]. This was followed by the 80ns fast relaxation measured to have a ΔV = -3ml mol^{-1} and a ΔH = -3kcal mol^{-1}. The authors assigned this phase to CO migration from the primary docking site or a Xe docking site to another Xe docking site. Migration of the ligand out of the distal pocket reduces repulsive interactions between the CO oxygen and the N_ε hydrogen of His64 significantly contributing to the overall observed relaxation [35]. Subsequent to the prompt 80 ns phase, Angeloni and Feis observed an ~800ns phase with ΔH_{struc}~11kcal mol^{-1} and ΔV_s 3 ± 1 ml mol^{-1} assigned to the protein motions, including breakage of a salt bridge between Lys45 and the heme 6-propionate group, opening an access channel for CO to escape to the surrounding solvent and a subsequent water molecule to enter the protein matrix [32].

5. Photoacoustic studies of photo-induced spin relaxation

The ability to modulate the spin-state within a transition metal complex is of significant interest for the design of novel magnetic materials. Of specific interest is the ability to switch between metal spin-states using optical triggering at room temperature. Several metal complexes have now been synthesized utilizing isomerizable 'push-pull'

ligands in which the field strength of the ligand can be modulated either thermally or through photonics. These complexes are of the $Fe^{II}(L_4)(X_2)$ type or $Fe^{III}(L'_4)(L)(X)$ type in which L is the push-pull ligand. An example of this type of complex utilizes L = 4-sterylpyridine (Stpy) (1-phenyl-2-(4-pyridyl) ethane) as well as several phenyl derivatives to photo-induce the spin crossover [43-45]. It has been shown that the Fe^{II}(*trans* $Stpy)_4(NCS)_2$ complex undergoes a thermally induced high-spin to low-spin transition with a cross over temperature centered near 190 K [43]. Subsequent photoexcitation of this complex imbedded within a cellulose acetate substrate results in a *trans* to *cis* isomerization of the Stpy which also induces the high-spin to low-spin transition at 140K.

The drive to produce transition metal complexes with photo-induced spin crossovers at high temperatures has led to the synthesis complexes such as $[Fe^{III}(salten)(mepepy)]BPh_4$ (mepepy = 1-(pyridin-4-yl)-2-(N-methylpyrrol-2-yl)-ethene; salten = 4 -azaheptamethylene- 1,7 bis(salicylideneiminate)) (Fig. 9). This complex has been shown to exhibit a photo-induced high-spin to low-spin transition at room temperature [44-46]. The mepepy ligand associated with the Fe(III)(salten)(mepepy) complex (Fig. 9) is a push-pull type molecule that exhibits either a *cis* or *trans* conformation and contains an electron-withdrawing pyridyl group and an electron-donating N-methylpyrrole group, separated by an photo-isomerizable double bond. Although the *trans* to *cis* photo-isomerization process is effective in modulating the ligand field strength due to changes in basicity much less is known about the electronic properties and energetics of this process. The ability to photo-initiate a spin-crossover in the Fe(III)(salten)(mepepy) complex affords a unique opportunity to probe the thermodynamics of this process at room temperature in solution. Enthalpies of spin-crossover complexes have been measured on powder or single crystal samples at T< 300K). Differential scanning calorimetry (DSC) indicates enthalpies of < 1 kcal mol^{-1} for the spin state transition that are coupled to small structural changes [47-49]. As an example of such spin state changes, the thermally induced low-spin to high spin transition in Fe(II) tris(2-(2'-pyridyl) benzimidazole) occurs with a transition temperature of 140K and an enthalpy change of 0.6 kcal mol^{-1} and is accompanied by an overall increase in unit cell volume [48]. More recently, thermal and photoinduced spin crossover in novel 3D metal organic materials was examined in both bulk materials and thin films revealing small enthalpy changes ranging from ~ 1 to ~ 4 kcal mol^{-1} at temperatures below 300K [50].

Recently, our laboratory has utilized PAC and computational methods to probe the energetics associated with both the *trans* to *cis* photo-isomerization of mepepy and as well as the high-spin to low-spin transition in the Fe(III)(salten)(mepepy) complex [51, 52]. Density functional

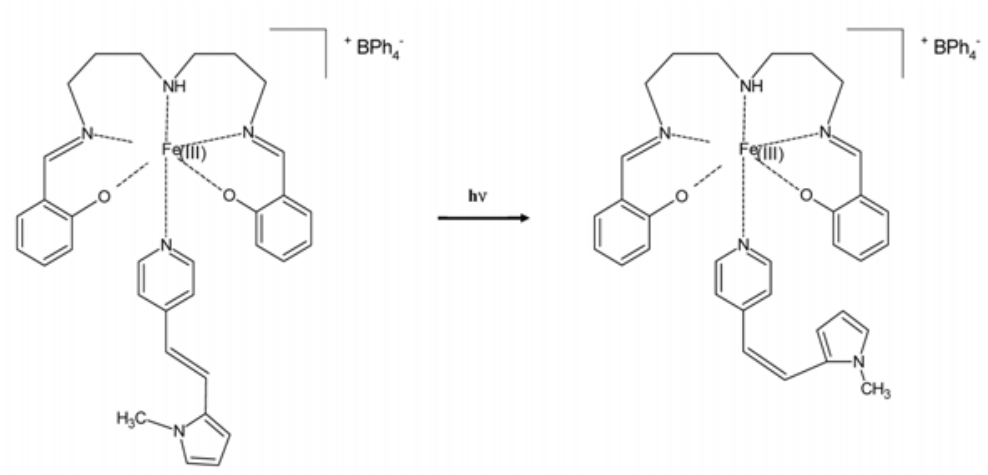

Fig. 9. The Fe(III)(salten)(mepepy) complex.

theory calculations demonstrate a global energy difference between *cis* and *trans* isomers of mepepy to be 8 kcal mol^{-1} while a slightly lower energy is observed between the local minima for the *trans* and *cis* isomers (7 kcal mol^{-1}) [52]. Interestingly, the *trans* isomer appears to exhibit two ground state minima separated by an energy barrier of ~9 kcal mol^{-1}.Results from the PAC studies indicate that the *trans* to *cis* isomerization results in a negligible volume change (0.9 ± 0.4 ml mol^{-1}) and an enthalpy change of 18 ± 3 kcal mol^{-1}. The fact that the acousticwaves associated with the *trans* to *cis* transition of mepepy overlap in frequency with those of a calorimetric reference implies that the conformational transition occurs faster than the ~50 ns response time of the acoustic detector. The observed volume change has contributions from changes in van der Waals volume of the mepepy molecule subsequent to isomerization and to electrostriction effects associated with changes in overall charge due to shifts in the ground-state dipole moment. The volume change due to electrostriction can be estimated using [53, 54]:

$$\Delta V_{elec} = -\left(\frac{\Delta\mu^2}{r^3}\right)\kappa_T\left[\frac{(\varepsilon+2)(\varepsilon-1)}{(2\varepsilon+1)^2}\right]\left(\frac{N_A}{4\pi\varepsilon_o}\right) \quad (15)$$

where Δμ is the change in dipole moment upon isomerization, *r* is the cavity radius of the molecule, κ_T is the compressibility of the solvent, ε is the solvent's dielectric constant, N_A is Avogadro's number, and ε_o is the vacuum permittivity. Using the previously calculated dipole change for the *trans* to *cis* isomerization of 0.0398 D [51], a molecular radius of ~5 Å (this assumes the mepepy molecule sweeps out a sphere of diameter ~10 Å), the electrostriction volume change was calculated to be ~-0.2 mL mol^{-1}. The corresponding van der Waals volume change between the *trans* and *cis* isomers was previously estimated to be $\Delta V_{cis\text{-}trans}$ ~ 9 mL mol^{-1} [51] giving a total ΔV (i.e., van der Waals volume changes and the electrostriction change) of ~ −9.2 mL mol^{-1} which is significantly lower than the observed ΔV = 0.7 mL mol^{-1} indicating additional contributions to the volume change must be present.

The change in molar volume in this case was rationalized by the loss of a hydrogen bond between a solvent water molecule and the N atom associated with the pyridine ring of the mepepy. In water the *trans* form of mepepy exhibits an absorption band at 425 nm which is not present in basic solutions. Thus, this band arises from a HOMO to LUMO transition for a mepepy molecule containing a hydrogen bonded/protonated N atom on the pyridyl unit. Upon photoisomerization to the *cis* isomer the electron density on the N atom is reduced resulting in a loss of the H-bond between a water molecule and the mepepypyridyl group. Van Eldik *et al.* have suggested that, on average, bond cleavage reactions increase the molar volume by ~ 5-10 mL mol^{-1} which together with the electrostriction volume and van der Waals volume changes accounts for the observed volume change [3]. Thus, it is apparent that the *trans* conformation of mepepy solubilized in acetonitrile:water retains the protonation/hydrogen bonding to the pyridyl N atom and that this interaction is lost upon isomerization to the *cis* conformation.

The corresponding change in enthalpy, obtained from the PAC results is 18 kcal mol^{-1}. In contrast, the results of the computational studies suggest an energy difference of only ~8 kcal mol^{-1} between the global energy minima between the *cis* and *trans* conformers. The ~10 kcal mol^{-1} difference in energies must also be due to distinct interactions between the mepepy conformers and the aqueous solvent. Previous studies of hydrogen bonding interactions between water and pyridine have shown that the hydrogen bond energy is on the order of 6-8 kcal mol^{-1}, very near the difference observed between the theoretical energy difference and that observed from PAC [55-57]. Thus, the change in enthalpy between the *cis* and *trans* conformers is also consistent with the loss of a hydrogen bond between water and the pyridine N subsequent to the isomerization.

5.1. Saltenmepepy complex

The results of the PAC studies also indicate that the mepepy *trans* to *cis* isomerization and associated spin crossover of the Fe(III)(salten)(mepepy) occurs in < ~ 50 ns as evident from the lack of frequency shift between the PAC signals of the complex and the calorimetric reference. From a plot of $\phi E_{h\upsilon}$ versus ($C_p\rho/\beta$) (Fig. 10), the volume and enthalpy changes are determined to be ΔV = 0.9 ± 0.3 mL mol^{-1} and ΔH = 37 ± 10 kcal mol^{-1}. The observed volume change has contributions from the *trans* to

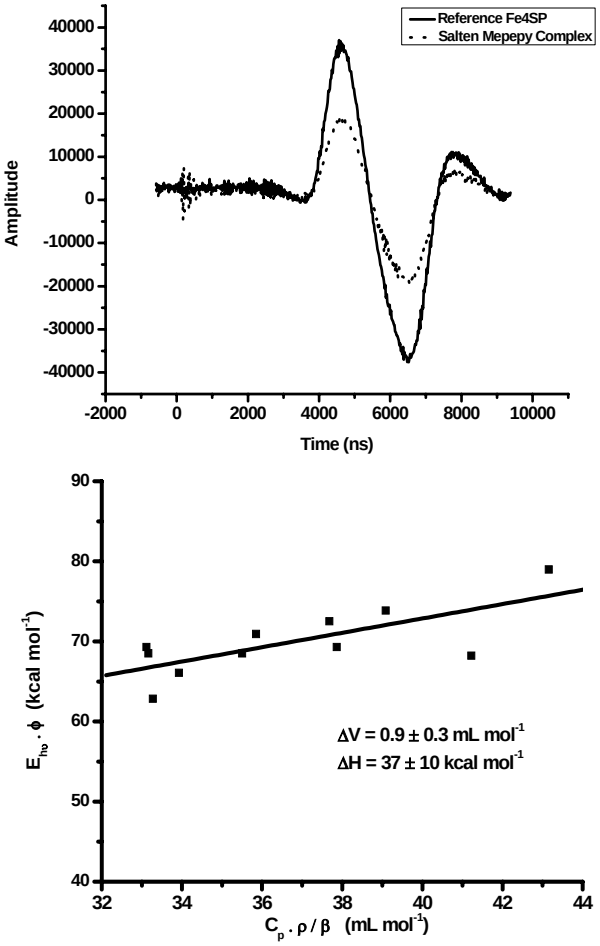

Fig. 10. Top- Overlay of photoacoustic traces for a calorimetric reference (solid) and the Fe(III)(salten)(mepepy) complex (dotted line). Bottom- Corresponding plot of $E_{hv}\phi$ versus ($C_p\rho/\beta$).

cis isomerization of the mepepy (discussed above) as well as the spin crossover of the Fe(III) ion. In order to extract the volume change associated with the spin crossover, the volume change associated with the mepepy isomerization must be subtracted from the overall volume change. However, as the N-atom of the pyridine group is coordinated to the iron atom (precluding H-bonding interactions with the solvent) only the previously estimated van der Waals and electrostriction contributions are included i.e.,~ -9.3 mL mol^{-1} . Thus, the volume change of the iron spin is then estimated to be ~10.2 mL mol^{-1}. Interestingly, high pressure studies of several Ni and Fe ligand complexes have suggested that volume change associated with a low- to high-spin transition is on the order of ~ 10 mL mol^{-1} [3]. This value was attributed to expansion of the metal-ligand core as well as electron repulsion between the $3d_{z_2}$ orbitals and ligand σ orbitals. Since the Fe(III)(salten)(mepepy) complex examined here undergoes a high-spin to low-spin a ΔV of ~ -10 mL mol^{-1} would be expected.

The difference in the observed volume change between previously reported metal complexes and the Fe(III)(salten)(mepepy) may be due to a significant distortion of the complex following the central iron spin state change resulting in cleavage of one or more of the Fe-L bonds. Such a spin state induced bond cleavage has been observed previously for a dicyano [2,13-dimethyl-6,9-dioxa-3,12,18-triazabicyclo [12.3.1] octadeca-1(18),2,12,14,16-pentaene] Fe(II)monohydrate complex ([Fe(II)L$(CN)_2$)]●H_2O) which undergoes both an optically/ thermally induced spin state change in the solid state in the temperature range from ~125-150K [58]. In the high spin state [Fe(II)L$(CN)_2$)]●H_2O exhibits pentagonal bipyramidal geometry with a hepta-coordinate ligation around the central iron which, upon conversion to the low spin state, becomes hexa-coordinate via the loss of an oxygen ligand. In the case of the Fe(III)(salten)(mepepy) complex examination of the average Fe···O and Fe···N bond distances reveals that the axial Fe···N bond to the secondary amine has a higher average bond length indicating a lower bond energy [59]. Thus, it is possible that cleavage of the Fe-N bond could occur within the complex upon spin crossover accounting for the difference in the observed ΔV between Fe(III)(salten)(mepepy) and other metal complexes Pixton *et al.* calculated a ΔV ~24 mL mol^{-1} for the cleavage of a Fe···N bond between a histidine and heme which can be used to estimate the contribution of the bond cleavage to the volume change in the Fe(III)(salten)(mepepy) complex [60]. The release of the salten N-group would also result in solvent hydrogen bonding in the mixed acetonitrile-water system. The volume change for hydrogen bond formation has been estimated to be on the order of -10 mL mol^{-1} [61]. Considering the Fe-N bond cleavage step the overall $\Delta V_{obs} = \Delta V_{Fe\text{-}N} + \Delta V_{N\text{-}H} + \Delta V_{HS\text{-}LS}$ (after subtracting ΔV_{mepepy}) which gives $\Delta V_{HS\text{-}LS} = \Delta V_{obs} - \Delta V_{Fe\text{-}N} - \Delta V_{N\text{-}H}$ = 10 mL mol^{-1} – 20 mL mol^{-1} + 10 mL mol^{-1} ~0 mL mol^{-1}. The lack of any significant volume change due to the spin state

transition is consistent with the fact that, other than the loss of the Fe-N coordination, the iron retains all of the other ligands precluding any electronic repulsion between the Fe $3d_{z^2}$ orbital and solvent molecules. This hypothesis is also consistent with volumetric studies of the volume change of spin crossover within the crystal forms of various iron complexes that show an average of volume change between 2-3 $Å^3$ which correspond to a volume change of only 1-2 mL mol^{-1} [62, 63].

The corresponding enthalpy change has contributions from the *trans* to *cis* isomerization of the mepepy ligand as well as the spin state change of the iron and any changes in core conformation such that $\Delta H_{obs} = \Delta H_{mepepy} + \Delta H_{Fe\text{-}N} + \Delta H_{N\text{-}H} + \Delta H_{HS\text{-}LS}$. The theoretical enthalpy value for the *trans* to *cis* isomerization of the mepepy ligand was calculated to be ~8 kcal mol^{-1} [51]. Subtracting this value from the observed enthalpy gives ~ 29 kcal mol^{-1} for the subsequent Fe-N bond cleavage, hydrogen bond formation and corresponding spin state change (i.e., $\Delta H_{obs} - \Delta H_{mepepy} = \Delta H_{Fe\text{-}N} + \Delta H_{N\text{-}H} + \Delta H_{HS\text{-}LS}$). Previous studies have further demonstrated that hydrogen bonds between water and pyridine have a bond energy on the order of ~6-8 kcal mol^{-1} [64-66] while those between water and dimethylamine are on the order of 5-6 kcal mol^{-1} [67]. By taking into account the formation of H-bond between a water molecule and the secondary amine (exothermic), the remaining difference between the theoretical and experimental values is ~ 35 kcal mol^{-1} (i.e., 35 kcal mol^{-1} = $\Delta H_{obs} - \Delta H_{mepepy} - \Delta H_{N\text{-}H} = \Delta H_{Fe\text{-}N} + \Delta H_{HS\text{-}LS}$). Finally, the enthalpy of dissociation of an Fe···N bond from Fe-NH_3 type complexes is on the order of ~ 30 kcal mol^{-1} [68] which results in a $\Delta H_{HS\text{-}LS}$ of ~ 5 kcal mol^{-1} which is negligible when considering the experimental uncertainty.

6. Photoacoustic studies of Ru(II)tris-(2,2'-bipyridine) in aqueous and micellar media

Coordination complexes involving d^6 transition metals, such as ruthenium, and nitrogen containing ligands have been the subject of a large body of research over the past thirty years due to their unique photophysical properties. In particular, coordination complexes of ruthenium and N-heteroaromatic ligands (e.g. 2,2'-bipyridine, bpy, or 1,10-phenanthroline, phen) typically exhibit long-lived excited states (~100ns-~10μs depending on the solvent environment) with appreciable fluorescence quantum yields (~0.04-0.1). One of the most widely studied compounds within this subset is [tris-(2,2'-bipyridine)]ruthenium(II), $Ru(II)(bpy)_3$, and will be the focus of the discussion below.

The absorption spectra of $Ru(II)(bpy)_3$ contains a number of transitions throughout the ultraviolet and visible regions corresponding to ligand centered π-π* (~280nm, ε ~ 80 mM cm^{-1}), metal centered, Laporte forbidden d-d (~333nm, ε ~ 2 mM cm^{-1}), and metal-to-ligand charge transfer (MLCT) (~450nm, ε ~ 12 mM cm^{-1}) transitions (Fig. 11).

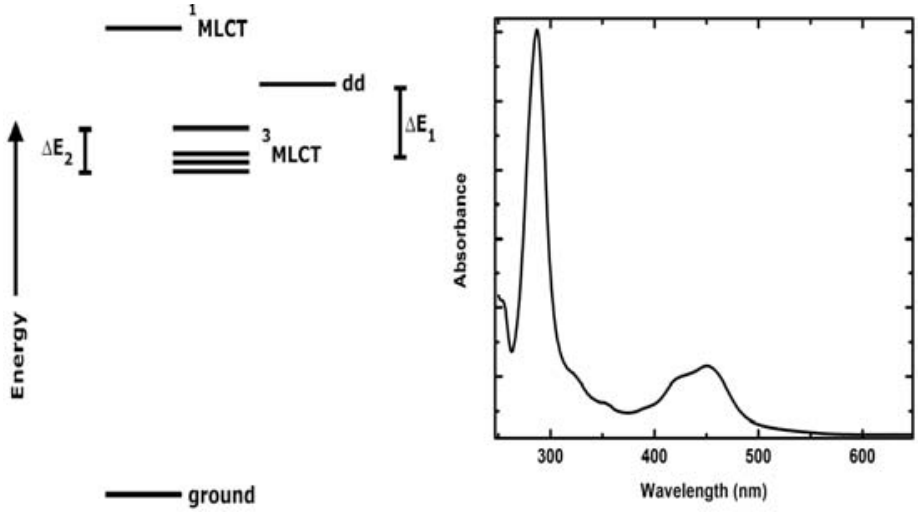

Fig. 11. State diagram for $Ru(bpy)_3$, left, and steady-state absorption spectra of $Ru(bpy)_3$ (in ethanol), right.

Excitation of the Ru(II)(bpy)$_3$ via any of these optical transitions results in the generation of a singlet MLCT state, ^{1}MLCT, that is strongly spin-orbit coupled to one of three lower-lying nearly degenerate triplet MLCT states, ^{3}MLCT. The degree of spin-orbit coupling is such that the quantum yield for the otherwise spin-forbidden transition from ^{1}MLCT to ^{3}MLCT is near unity and occurs on a picosecond timescale. At room temperature the three close lying ^{3}MLCT states are experimentally indistinguishable and are observed to have partial singlet character [69, 70].

Two remaining states have been identified lying slightly higher in energy than the three lower-lying ^{3}MLCT states including a fourth ^{3}MLCT of more singlet character and a ^{3}dd state. The degree to which these states are thermally populated is related to the energy gap between these states and the low-lying ^{3}MLCT. The energy gaps can be experimentally determined by the temperature dependence on the observed excited state decay rates via the expression:

$$k_{obs} = k_o + k_1 exp\left[-\frac{\Delta E_1}{kT}\right] + k_2 exp\left[-\frac{\Delta E_2}{kT}\right] \quad (16)$$

where k_o is the sum of the temperature independent radiative and non-radiative decay rates for the transition from the low-lying ^{3}MLCT to the ground state, k_1 and k_2 are the decay rates back to the ground states from the fourth ^{3}MLCT (~10^7-10^9 s^{-1}) and ^{3}dd state (~10^{12}-10^{14} s^{-1}) respectively and ΔE_1 and ΔE_2 are the energy gaps between the low-lying ^{3}MLCT and either the fourth ^{3}MLCT (~100-1000 cm^{-1}) and ^{3}dd (~2500-4000 cm^{-1}) respectively [71, 72] (Fig. 11). However, the third term corresponding to the ^{3}MLCT→^{3}MLCT transition is typically only non-zero at low temperatures in glassy matrices. Thus under solution conditions near room temperature the temperature dependence of the observed decay rate is reduced to:

$$k_{obs} \approx k_o + k_1 exp\left[-\frac{\Delta E_1}{kT}\right] \quad (17)$$

6.1. Photoacoustic calorimetric studies of Ru(II) complexes in solution

PAC analysis of the photophysics and photochemistry, including excited state redox reactions, of Ru(II)(bpy)$_3$ and other Ru(II)(bpy)$_3$ derivatives have been carried out in aqueous solution (Fig. 12) [73-76]. Excitation of Ru(II)(bpy)$_3$ results in a fast (<50ns) volume contraction of ~3 mL mol^{-1} corresponding to the picosecond formation of a ^{3}MLCT excited state and is thought to be dominated by structural changes related to both lengthening of the Ru-N bonds and electrostriction due to the formation of an excited state dipole [73, 77, 78]. The observed fast contraction is accompanied by an enthalpy change of 45 kcal mol^{-1} (after scaling for the quantum yield) which matches the energy of the emission maxima (627nm, 46 kcal mol^{-1}) [79].

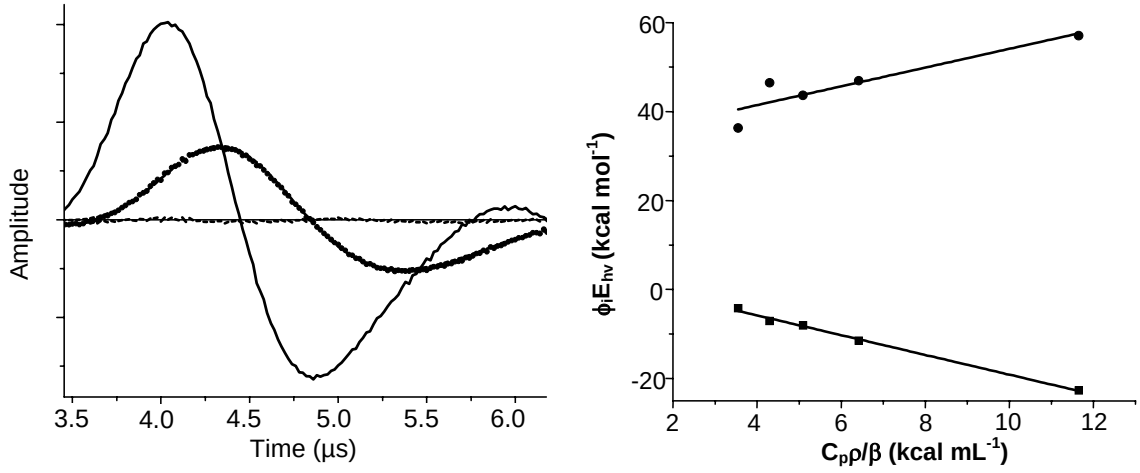

Fig. 12. (left) Deconvolution fit (dashed line) of PAC signal (circles) for Ru(II)(bpy)$_3$ in pure water at 34°C. (right) Plot of ϕ obtained by deconvolution as a function of the thermodynamic solvent properties of water, $C_p\rho/\beta$, which are very temperature dependent.

An additional ~600 ns phase has been observed in the PAC signal corresponding to the spin-forbidden depopulation of the ^{3}MLCT to the singlet ground state with a lifetime that is in very good agreement with previously observed emission lifetime (Fig. 12) [80]. The 600ns phase is accompanied by a volume expansion of ~3 mL mol^{-1} and an enthalpy change of ~-46 kcal mol^{-1} which is consistent with the relaxation of the excited state in the absence of any side reactions [73, 75, 76]. The decay rate observed by PAC (Fig. 13) displays a moderate temperature dependence. Fitting the data to Eq. 17 results in a k_o of 7x10^5 s^{-1}, k_1 of 1.6x10^{12} s^{-1}, and a ΔE_1 of 2993 cm^{-1} (previously unpublished) which is in excellent agreement with values previously obtained from emission lifetime measurements (k_o = 6x10^5 s^{-1}, k_1 = 4x10^{12} s^{-1}, ΔE_1 = 3275 cm^{-1}) [81].

In the presence of a suitable quencher, the Ru(II)(bpy)$_3$^{3}MLCT is known to undergo oxidation via excited state electron transfer [74, 75, 82]. For example, in the presence of varying concentrations of methyl viologen (MV^{2+}) the observed enthalpy and volume changes occurring in the fast phase are unaffected by the presence of MV^{2+} [74]. The rate of the slow phase was observed to increase with increasing concentration of MV^{2+}. The increase in decay rate of the ^{3}MLCT state was accompanied by a decrease in the enthalpy change observed in the absence of MV^{2+}. The decrease in the decay rate with the accompanying enthalpy and volume changes were attributed to the forward electron transfer (ET) reaction between the Ru(III)(bpy)$^{\bullet-}$(bpy)$_2$ and MV^{2+} contact pair and subsequent escape of the newly formed ion radicals from their solvent cage according to:

$$\boldsymbol{Ru(III)(bpy)_2(bpy^{\cdot-})\cdots MV^{2+} \rightarrow Ru(III)(bpy)_3\cdots MV^{\cdot+} \rightarrow Ru(III)(bpy)_3 + MV^{\cdot+}}$$

where the charge separation between $MV^{\cdot+}$ and Ru(III)(bpy)$_3$ occurs with an efficiency, ϕ_{CS}, of 0.25 in aqueous solutions [83-85]. The observed enthalpy change for this slow phase can then be described as:

$$\Delta H_{obs} = \Phi_{MLCT}[1-\phi_{ET}(1-\phi_{CS})-\phi_{ET}]\Delta H_{MLCT} + \phi_{CS}\phi_{ET}\Delta H_{CS} \quad (18)$$

where Φ_{ET} is the efficiency of quenching of the ^{3}MLCT state by MV^{2+} at the given concentration according to:

$$\phi_{ET} = \frac{k_q\tau_o[MV^{2+}]}{1+k_q\tau_o[MV^{2+}]} \quad (19)$$

where k_q is the rate constant for the oxidative quenching of the ^{3}MLCT state by MV^{2+}, and τ_o is the excited state lifetime of Ru(II)(bpy)$_3$ in the absence of MV^{2+}. It should be noted that equation 18 assumes that the energy loss due to excited state emission is negligible (i.e., $\Phi_{fl}E_{fl}$~ 3 kcal mol^{-1}) which is reasonable within the experimental error of the PAC measurements. Considering that the quantum yield for the formation of the ^{3}MLCT is approximately unity, simplification of eq. 18 yields an expression for the enthalpy change in terms of the concentration of MV^{2+}:

$$\Delta H_{obs} - \Delta H_{MLCT} = \left(\frac{k_q\tau_o[MV^{2+}]}{1+k_q\tau_o[MV^{2+}]}\right)\phi_{CS}\Delta H_{CS} - \left(\frac{k_q\tau_o[MV^{2+}]}{1+k_q\tau_o[MV^{2+}]}\right)\Delta H_{MLCT} \quad (20)$$

A fit to the [MV^{2+}] dependent data provided in reference 74 as a function of [MV^{2+}] indicate that the enthalpy change associated with the formation of the solvated ion pair, ΔH_{CS}, is approximately 71 ± 4 kcal mol^{-1} (see Fig. 14). This value is 10 kcal mol^{-1} less than the value given in reference 74 (81 ± 5 kcal mol^{-1}). It should be noted that the value reported was calculated as an average value of the individual points over the concentration range of MV^{2+} according to:

$$\Delta H_{CS} = \frac{E_{h\nu} - Q_{prompt} - Q_{slow} - \left(1-\phi_{ET}\right)\phi_{em}E_{em}}{\eta_R} \quad (21)$$

where each term has the same meaning as above: $E_{h\nu}$ is the energy of the incident photon and η_R is defined as the product of the quantum yield for intersystem crossing (stated earlier as being unity), the efficiency of quenching (ϕ_{ET}), and the probability for the free radical escape from the contact pair solvent cage (0.25). Similarly, the change in molar volume can be expressed as:

$$\Delta V_{obs} - \Delta V_{MLCT} = \left(\frac{k_q \tau_o [MV^{2+}]}{1 + k_q \tau_o [MV^{2+}]}\right) \phi_{CS} \Delta V_{CS} - \left(\frac{k_q \tau_o [MV^{2+}]}{1 + k_q \tau_o [MV^{2+}]}\right) \Delta V_{MLCT} \quad (22)$$

which, when fit to the data provided in ref 74, gives a volume change associated with the formation of the charge separated ion pair, ΔV_{CS}, of 18 ± 3 mL mol^{-1}. This value is nearly twice the magnitude of the reported value which utilized single data points to determine the change in volume (~10 ± 1 mL mol^{-1}).

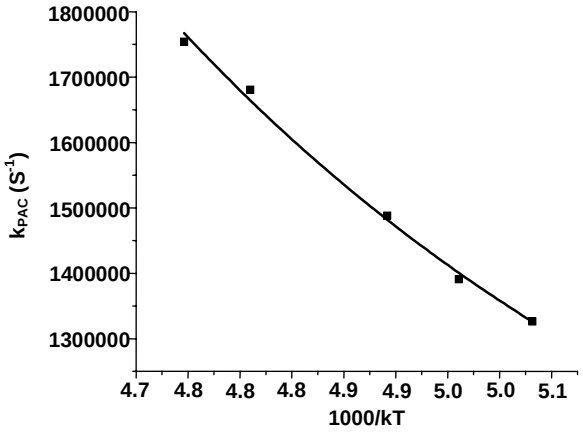

Fig. 13. Temperature dependence of the decay rates of the second phase observed by PAC for Ru(II)(bpy)$_3$ in water (λ_{exc} = 532nm). Data was fit to equation 17.

The estimated volume change upon forward ET with concomitant charge separation is significantly larger (and opposite in sign) than that expected for solvent reorientation due to changes in electrostriction estimated using the Drude-Nernst equation:

$$\Delta V_{elec} = -B\frac{z^2}{r} \quad (23)$$

where B is an empirically determined parameter related to the solvent dielectric (~4.7 in water for cations and ~19 for anions), z is the unit charge on the species and r the radius (using a hard-sphere model and expressed in Å) [86, 87]. The discrepancy between the observed and calculated volume change was attributed to the limitations of using equation 23 due to: 1) inaccurate values for the B term in water and 2) the use of a hard-sphere model in expressing the radius of non-spherical molecules. It is important to note that

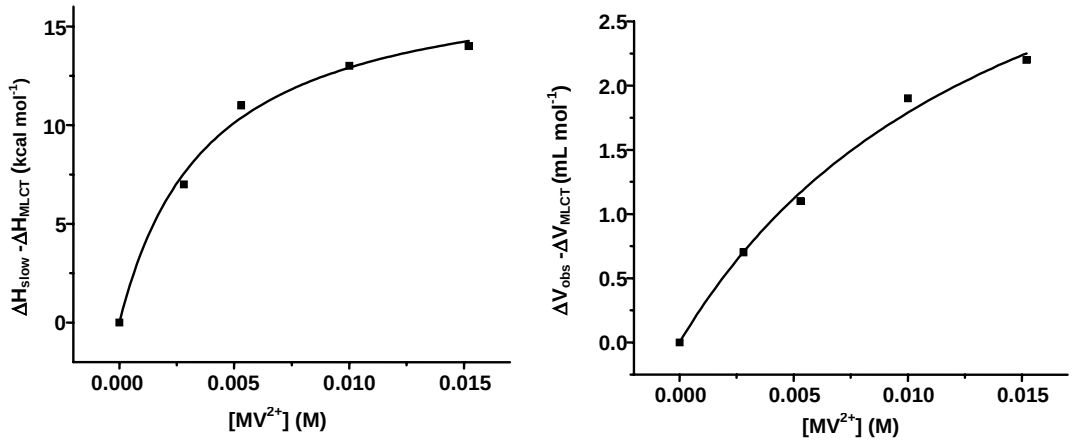

Fig. 14. Difference in the observed enthalpy changes for the decay of Ru(II)(bpy)3 in varying concentrations of MV^{2+} and the enthalpy change of the ^{3}MLCT in the absence of MV^{2+} (left) and volume changes for the same (right). Fits to the data were obtained using eq 20 and 22 respectively. Data taken from ref 74.

the calculated values in reference 72 were found using B equal to 4.175, r_{Ru} = 4.8Å and r_{MV} = 3.3Å; although, using B = 4.7, r_{Ru} = 7Å and r_{MV} = 3.3Å still results in a large discrepancy between observed and calculated values [88-90]. Changes in volume due to structural variations were not significant based upon crystallographic results and ESR data [91, 92].

6.2. Reverse micelles as a method of controlling salvation

Reverse micelles (RM) are suspensions of amphiphilic surfactant molecules comprised of a polar "head" group and non-polar "tail" in non-polar media that spontaneously self-aggregate forming nanostructures (or nano-vesicles) in the presence of water. The size of the RM nanodroplet is directly dependent on the water content in solution described in terms of the concentration ratio of water to surfactant, $w_o = [H_2O]/[surfactant]$. Naturally, the size of the interior water pool is directly proportional to w_o and increases with an increasing value of w_o.

The water pool located on the interior (Fig. 15) of these "water-in-oil" microemulsions contain a region at the water-surfactant interface in which the behavior of water differs from that of bulk water whereas the properties of the water core approach those of bulk water near the center of the pool [93-95]. The origin of the reduced "bulk" behavior at the interfacial region has been attributed to decreased water-water interactions due to increased water-surfactant interaction (which includes interactions with the surfactant head-group as well as surfactant counter ions also present within the RM) [96, 97]. Molecular dynamics studies of the behavior of water within RM with increased w_o indicate that an increase in the water content within the RM, accompanied by a decrease in the interfacial charge density, expands the hydrogen-bonding network within the RM leading to more bulk-like behavior [98, 99]. These properties make RM solutions ideal model systems to probe the effects of confinement on volume changes related to structural changes and electrostriction.

6.3. Photoacoustic calorimetry studies on $Ru(II)(bpy)_3$ and derivatives in reverse micelle solutions

Previous PAC experiments involving RM solutions have examined the excited state properties of the $Ru(II)(bpy)(CN)_4^{2-}$ complex within dioctyl sodium sulfosuccinate (AOT) reverse micelles in alkanes [100-102]. Analysis of the photoacoustic data revealed that, in pure water, excitation of $Ru(II)(bpy)(CN)_4^{2-}$ resulted in a volume expansion of approximately 14 mL mol^{-1} with a corresponding enthalpy change of ~52 kcal mol^{-1} (τ < 50ns) consistent with the formation of the ^{3}MLCT state (47 kcal mol^{-1} at the emission maxima of 611nm) and is followed by a 100ns relaxation process with volume and enthalpy changes equal and opposite to those of the fast prompt (< 50ns) phase [100, 103].

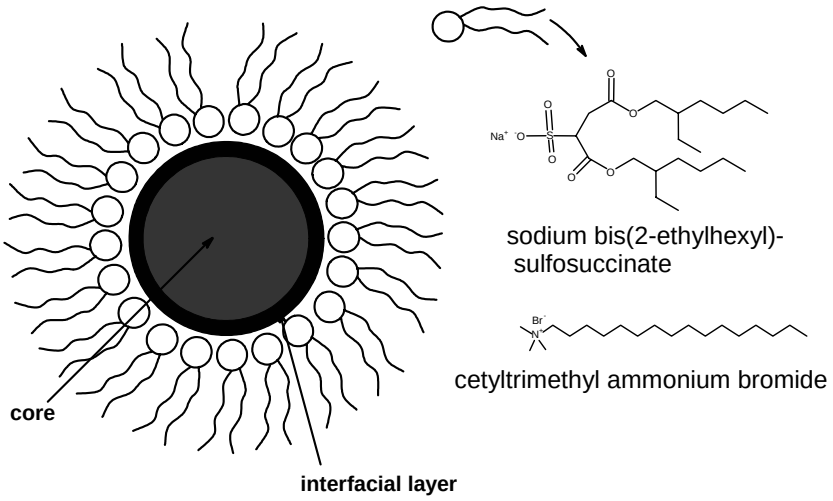

Fig. 15. Schematic representation of a reverse micelle nanostructure.

The expansion observed with the formation of the ^{3}MLCT was attributed to the weakening of hydrogen bonding to the cyano groups due to reduced π back bonding decreasing the electron density on the CN^- group [100].

The observed enthalpy change is unaffected with varying concentrations of water and is within experimental error of the value observed in neat water. The volume expansion observed for the formation of the ^{3}MLCT was shown to decrease with water content (decreasing w_o). Lifetimes for the relaxation of the ^{3}MLCT extracted from deconvolution of the PAC signal increased with decreasing w_o. This slower relaxation with decreasing water content was accompanied by a volume contraction that was equal and opposite to the corresponding volume expansion at the given w_o value.

Overall, the observed results can be interpreted as arising from the differences in the hydrogen-bonding network between "bulk" water and the water pool within RM of w_o values < 10. At lower water content the degree to which water molecules hydrogen-bond and the strength of those interactions are believed to be significantly weaker due to competing interactions with the charged surfactant head groups and counter ions diminishing the number of solvent vibrational modes available to couple with the ^{3}MLCT, in turn, decreasing the non-radiative component of the excited state lifetime. The weaker water-water interactions at lower w_o may also explain the observed decrease in the solvent rearrangement upon decreased hydrogen-bonding with the formation of the Ru(II)(bpy)$(CN)_4^{2-3}$MLCT.

Interestingly, preliminary results from our laboratory for Ru(II)$(bpy)_3$ in cationic CTAB RM in decane using hexanol as a co-solvent (w_o =18) are somewhat contradictory (Fig. 16). Upon formation of the ^{3}MLCT the enthalpy change observed resembles that of Ru(II)$(bpy)_3$ in water and is reversible. However, the volume changes observed for the formation and decay of the ^{3}MLCT (-6±5 mL mol^{-1} and 13±7 mL mol^{-1} respectively), although indicative of a reversible process, differ significantly from that of Ru(II)$(bpy)_3$ in water (~3 mL mol^{-1}). Analysis of the temperature dependence of the observed lifetimes (Fig. 17) also indicate that the ^{3}MLCT-^{3}dd energy gap is not significantly perturbed at the w_o used in the experiment (ΔE_1 = 2570 cm^{-1}). The decay rates obtained from the fit for the relaxation from the ^{3}MLCT (k_o = 13.1x10^5 s^{-1}) and ^{3}dd (k_1 = 1.0x10^{11} s^{-1}) manifolds are significantly different from those observed in water (see above). The decreased rates may be easily explained by reduction of the non-radiative coupling with the surrounding "solvent" due to weaker solvent-solvent interactions.

It might be expected that the magnitude of the volume change associated with the Ru(II)$(bpy)_3$ formation/decay would decrease due to restricted solvent rearrangement arising from a weaker solvent-solvent hydrogen-bonding network. It has

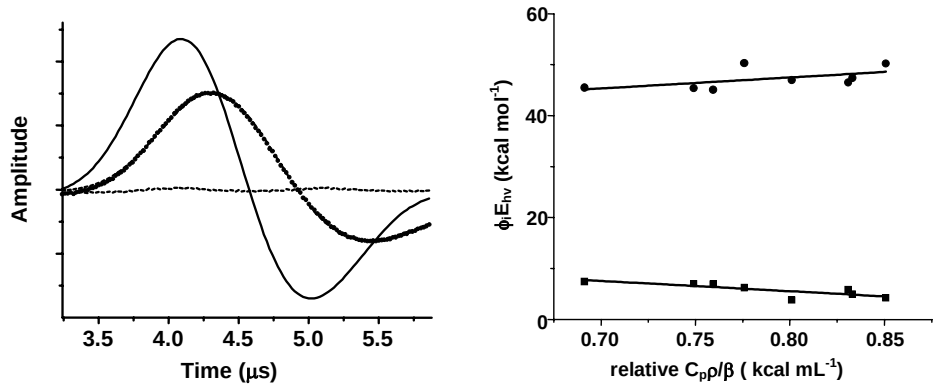

Fig. 16. (left) Deconvolution fit (dashed line) of PAC signal (circles) for Ru(II)$(bpy)_3$ in CTAB reverse micelle solution (w_o= 17.8) at 31°C. (right) Plot of ϕ obtained by deconvolution as a function of ratio of ref amplitude in water to ref amplitude in CTAB reverse micelle solution at various temperatures.

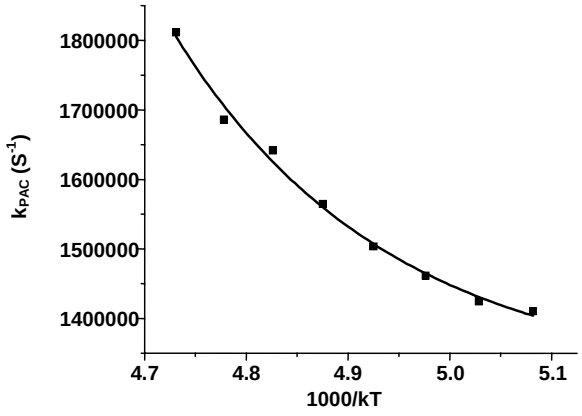

Fig. 17. Temperature dependence of the decay rates of the second phase observed by PAC for $Ru(II)(bpy)_3$ in a CTAB RM solution with w_o 17.8 (λ_{exc}=532 nm). Data was fit to equation 17.

been previously proposed that the volume change due to electrostriction of the solvent in immediate proximity of the ion can be related to the "solvent" compressibility, κ_T, by [104]:

$$\Delta V_{elec} = \int_r^{\infty} -\frac{\Delta V(r)}{V} 4\pi r^2 dr \qquad (24)$$

where the fractional change in volume is given by:

$$-\frac{\Delta V(r)}{V} = \int_0^{P(r)} \kappa dP \qquad (25)$$

Substitution of eq 25 into eq 24 yields

$$\Delta V_{elec} = \iint_{r,0}^{\infty,P(r)} (\kappa dP)(4\pi r^2 dr) \qquad (26)$$

In calculating the solvent parameters $C_p\rho/\beta$ and κ for the CTAB RM solution relative to bulk water, it was found that in the CTAB RM solution κ differed from that of water by a factor of approximately 1.2 on average. The volume change due to electrostriction upon formation of the ^{3}MLCT in the CTAB RM should differ by approximately the same factor. The above methods treat the "solute" as a point-charge within a dielectric continuum. The present situation is somewhat more complex in that the ^{3}MLCT is, in principle, a newly formed dipole inducing reorganization of the immediate surrounding solvent molecules which (depending on the distance and number of solvation layers between the dipolar "solute" and the surfactant head-group interface) may interact strongly with the already "rigid" interfacial water layer and/or the electric field of the charged surfactant interface [105].

Goodman and Herman [73], however, point out that electron exchange between the bipyridyl ligands occurs within picoseconds. Thus, on the time window of PAC, the electron density appears delocalized over the three bipyridine ligands and that the observed volume change is predominantly due to structural changes of the complex arising from elongation of the Ru-N bonds due to thermal population of the ^{3}dd state and the subsequent solvent reorganization about a structurally different transient. Within the CTAB RM this would imply that the observed volume change has at least two components: one due to reorganization of the water "solvent" about the structurally different transient and reorganization of the CTAB/decane/hexanol "solvent" about the structurally different water pool. Overall, the relationship between restricted solvent environment, electrostriction and excited state structural changes remain unclear and are the subject of further investigation in our laboratory.

SUMMARY

The ability to probe thermodynamics associated with physiological processes in biomolecules as well as photochemical process on sub-millisecond time scales remains a significant challenge in chemistry and biophysics. However, as demonstrated in the sections above, time resolved photothermal methods offer a unique opportunity to access enthalpy and molar volume changes associated with photo-initiated processes on time scales ranging from tens of milliseconds down to tens of nanoseconds. Photoacoustic calorimetry has now been widely applied to a vast array of chemical and biomolecular processes that can be photo-initiated and thermodynamic profiles have been revealed on very fast time scales. The PAC method can be applied to probe photo-triggered processes in both aqueous and non-aqueous solutions as well as processes in the solid state. Rapid advances in photo-chemical protecting group chemistry is opening entirely new avenues through which to utilize time resolved photothermal

methods to examine a much wider range of biomolecular processes including peptide and protein folding, cell signaling, protein-protein interactions and drug-protein interactions.

ACKNOWLEDGEMENTS

The Authors would like to acknowledge the National Science Foundation, the American Heart Association and the Department of Defense-Defense Threat Reduction Agency for support of this work.

REFERENCES

1. Lewis, G. N. and Randall, M. Thermodynamics, McGraw-Hill, Inc., NY 1961.
2. Hiromi, K. Kinetics of Fast Enzyme reactions: Theory and practice. Kodanshi Scientific Books: Kodanshi, Ltd. 1979.
3. van Eldik, R., Asano, T. and le Noble, W. J. 1989, Chemical Rev., 89, 549.
4. Vetromile, C. M., Miksovska, J. and Larsen, R. W. 2011, Biochim. Biophys. Acta., 1814, 1065-1076.
5. Miksovska, J., Norstrom, J. and Larsen, R. W. 2005, Inorg. Chem., 44, 1006-1014.
6. Barker, B. D. and Larsen, R. W. 2001, J. Inorg. Biochem., 85, 107-116.
7. Miksovska, J., Day, J. and Larsen, R. W. 2003, J. Biol. Inorg. Chem., 8, 621-625.
8. Larsen, R. W. and Langley, T. 1999, J. Am. Chem. Soc., 121, 4495-4499.
9. Hansen, K. C., Rock, R. S., Larsen, R. W. and Chan, S. I. 2000, J. Am. Chem. Soc., 122, 11567-11568.
10. Miksovska, J. and Larsen, R. W. 2003, J. Prot. Chem., 22**,** 387-394.
11. Chen, R. P-Y., Huang, J. J-T, Chen, H. L., Jan, H., Velusamy, M., Lee, C-T., Fann, W., Larsen, R. W., Chan, S. I. 2004, Proc. Nat. Acad. Sci., 101, 7305-7310.
12. Kuo, N. N-W., Huang, J. J-T., Miksovska, J., Chen, R. P-Y., Larsen, R. W., Chan, S. I. 2005, 127, 16945-16954.
13. Miksovska, J. and Larsen, R.W. 2007, Coord. Chem. Rev., 251, 1101-1127.
14. Patel, C. K. N. and Tam, A.C. 1981, Rev. Mod. Phys., 53, 517.
15. Jackson, W. B., Amer, N. M., Boccara, A.C. and Fournier, D. 1981, Appl. Optics, 20, 1333-1344.
16. Ort, D. R. and Parson, W. W. 1979, Biophys. J., 25, 355-364.
17. Rothberg, L. J., Simon, J. D., Bernstein, M. and Peters, K. S. 1983, J. Am. Chem. Soc., 105, 3464-3468.
18. Gensch T. and Viappiani C. 2003, Photochem. Photobiol. Sci., 2, 699-721.
19. Terazima M. 2002, J. of Photochem. Photobiol. C: Photochem. Rev., 3, 81-108.
20. Pettigrew, G. W. and Moore, G. R. Cytochromes c. Biological Aspects. Berlin - Heidelberg - New York: Springer Verlag 1987.
21. Dunford, H. B. Peroxidases and catalases: biochemistry, biophysics, biotechnology, and physiology, Hoboken, New Jersey, John Wiley & con, Inc., 2010.
22. Taylor, B. L. and Zhulin, I. B. 1999, Microbiol. Mol. Biol. Rev., 63, 479-506.
23. Huang, Y., Marden, M. C., Lambry, J. C., Fontaine-Aupart, M. P., Pansu, R., Martic, J. L. and Poyart, C. 1991, J. Am. Chem. Soc., 113, 9141-9144.
24. Cao, W., Ye, X., Sjodin, T., Christian, J. F., Demidov, A. A., Berezhna, S., Wang, W., Barrick, D., Sage, J. T., Champion, P. M. 2004, Biochemistry, 43, 7017-7027.
25. Collman, J. P. 1997, Inorg. Chem., 36, 5145-5155.
26. Blumenthal, D. C. and Kassner, R. J. 1980, J. Bio. Chem., 255, 5859-5863.
27. Cowley, A. B., Lukat-Rodgers, G. S., Rodgers, K. and Benson, D. R. 2004, Biochemistry, 433, 1656-1666.
28. Strickland, N. and Harvey, J. N. 2007, J. Phys. Chem. B, 111, 841-852.
29. Parsons, D. F. and Ninham, B. W. 2009, J. Phys. Chem. A, 113, 1141-1150.
30. Springer, B. A., Silgar, S. G., Olson, J. S. and Phillips, G. N. 1994, Chem. Rev., 94, 699-714.
31. Yang, F. and Phillips, G. N. 1996, J. Mol. Biol., 256, 762-774.
32. Angeloni, L. and Feis. A. 2003, Photochem. Photobiol. Sci., 2, 730-740.
33. Westrick, J. A. and Peters, K. S. 1990, Biophys. Chem., 37, 73.
34. Westrick, J. A., Peters, K. S., Ropp, J. D. and Sligar, S. G. 1990, Biochemistry, 29, 6741.

35. Goldbeck, R. A., Bhaskaran, S., Ortega, C., Mendoza, J. L., Olson, J. S., Soman, J., Kilger, D. S. and Esquerra, R. M. 2006, Proc. Natl. Acad. Sci. USA, 103, 1254-1259.
36. Leung, W. P., Cho, K. C., Chau, S. K. and Choy, L. 1987, Chem. Phys. Lett., 141, 220-224.
37. Kleinert, T., Doster, W., Leyser, H., Petry, W., Schwarz, V. and Settles, M. 1998, Biochemistry, 37, 717-733.
38. Sakakura, M., Yamaguchi, S., Hirota, N. and Terazima, M. 2001, J. Am. Chem. Soc., 123, 4286.
39. Frauenfelder, H., McMahon, B. H. and Fenimore, P.W. 2002, PNAS, 100, 8615-8617.
40. Ruscio, J. Z., Kumar, D., Shukla, M., Prisant, M. G., Murali, T. M. and Onufriev, A. V. 2008, Proc. Natl. Acad. Sci. USA, 105, 9204-9209.
41. Kitagawa, T., Haruta, N. and Mizutani, Y. 2002, Biopolymers, 67, 207-213.
42. Vetromile, C. M., Miksovska, J. and Larsen, R. W. 2011, Biochim. Biophys. Acta., 1814, 913-1106.
43. Boillot, M.-L., Roux, C., Audiere, J.-P., Dausse, A. and Zarembowitch, J. 1996, Inorg. Chem., 35, 3975.
44. Sour, A., Boillot, M.-L., Riviere, E. and Lesot, P. 1999, Eur. J. Inorg. Chem., 12, 2117.
45. Boillot, M.-L., Chantraine, S., Zarembowitch, J., Lallemand, J.-Y. and Prunet, J. 1999, New J. Chem., 23, 179.
46. Faulmann, C., Dorbes, S., Garreau de Bonneval, B., Molnar, G., Bousseksou, A., Gomez-Garcia, C. J., Coronado, E. and Valade, L. 2005, Eur. J. Inorg. Chem., 16, 3261.
47. Boca, R., Boca, M., Ehrenberg, H., Fuess, H., Linert, W., Renz, F. and Svoboda I. 2003, Chem. Phys., 293, 375.
48. Rodriguez-Velamazan, J. A., Castro, M., Palacios, E., Burriel, R., Sanchez Costa, J. and Letard, J. F. 2007, Chem. Phys. Lett., 435, 358.
49. Moliner, N., Carmen Munoz, M., Letard, S., Letard, J-F., Solans, X., Burriel, R., Castro, M., Kahn, O. and Real, J. A. 1999, Inorg. Chim. Acta, 291, 279.
50. Agusti, G., Cobo, S., Gaspar, A. B., Molnar, G., Moussa, N. O., Szilagyi, P. A., Palfi, V., Vieu, C., Munoz, M. C., Real, J. A. and Bousseksou, A. 2008, Chem. Mater., 20, 6721.
51. Mokdad, A., Belof, J. L., Wook, Yi, S., Shuler, S. E., Mc Laughlin, M. L., Space, B. and Larsen, R. W. 2008, J. Phys Chem. A, 112, 8310.
52. Mokdad, A. and Larsen, R. W. 2010, Inorg. Chimica. Acta, 363, 3338-3344.
53. Wegewijs, B., Paddon-Row, M. N. and Braslavsky, S. E. 1998, J. Phys. Chem. A, 102, 8812.
54. Padova, J. 1963, J. Chem. Phys., 39, 1552.
55. Papai, I. and Jansco, G. 2000, J. Phys. Chem. A, 104, 2132.
56. Zega, A., Srcic, S., Mavri, J. and Bester-Rogac, M. 2008, J. Mol. Struc., 875, 354.
57. Marczak, W., Lejmann, J. K. and Heintz, A. 2003, J. Chem. Therm., 35, 269.
58. Guionneau, P., Le Gac, F., Kaiba, A., Sanchez Costa J., Chasseau, D. and Letard, J-F. 2007, Chem. Comm., 36, 3723-3725.
59. Allen, F. H. 2002, Acta Crystallogr: Sect B, 58, 380.
60. Pixton, D. A., Petersen, C. A., Franke, A., van Eldik, R., Garton, E. M. and Andrew, C. R. 2009, J. Am. Chem. Soc., 131, 4846.
61. Oswal, S. L. 2005, ThermochimicaActa, 425, 59.
62. Guionneau, P., Marchivie, M., Bravic, G., Letard, J-F and Chasseau, D. 2002, J. Mater. Chem., 12, 2546.
63. Reger, D. L., Gardinier, J. R., Elgin, J. D., Smith, M. D., Hautot, D., Long, G. J. and Grandjean, F. 2006, Inorg. Chem., 45, 8862.
64. Papai, I. and Jansco, G. 2000, J. Phys. Chem. A, 104, 2132.
65. Zega, A., Srcic, S., Mavri, J. and Bester-Rogac, M. 2008, J. Mol. Struct., 875, 354.
66. Marczak, W., Lejmann, J. K. and Heintz, A. 2003, J. Chem. Therm., 35, 269.
67. Brink, G. and Glasser, L. 1982, J. Comp. Chem., 3, 47.
68. Riordan, C. G. and Halpern, J. 1996, Inorg. Chim. Acta, 243, 19.
69. Kober, E. M. and Meyer, T. J. 1982, Inorg. Chem., 21, 3967.

70. Xie, P., Chem, Y. J., Uddin, J. and Endicott, J. F. 2005, J. Phys. Chem. A., 109, 4671.
71. Barigelletti, F., Juris, A., Balzani, V., Beler, P. and Vonzelewsky, A. 1983, Inorg. Chem., 22, 3335.
72. Caspar, J. V. and Meyer, T. J. 1983, Inorg. Chem., 22, 2444.
73. Goodman, J. L. and Herman, M. S. 1989, Chem. Phys. Lett., 163, 417.
74. Borsarelli, C. D. and Braslavsky, S. E. 1999, J. Phys. Chem. A., 103, 1719.
75. Borsarelli, C. D., Corti, H., Goldfarb, D. and Braslavsky, S. E. 1997, J. Phys. Chem. A., 101, 7718.
76. Miksovska, J. and Larsen, R. W. 2004, Inorg. Chem., 43, 4051.
77. Bradley, P. G., Kress, N., Hornberger, B. A., Dallinger, R. F. and Woodruff, W. H. 1981, J. Am. Chem. Soc., 103, 7441.
78 Kirk, A. D., Hoggard, P. E., Porter, G. B., Rockley, M. G. and Windsor, M. W. 1976, Chem. Phys. Lett., 37, 199.
79. Demas, J. N. and Taylor, D. G. 1979, Inorg. Chem., 18, 3177.
80. Cherry, W. R. and Henderson, L. J. 1984, Inorg. Chem., 23, 983-986.
81. Allen, G. H., White, R. P., Rillema, D. P. and Meyer, T. J. 1984, J. Am. Chem. Soc., 106, 2613.
82. Jiwan, J. L. H., Chibisov, A. K. and Braslavsky, S. E. 1995, J. Phys. Chem., 99, 10246.
83. Magnuson, A., Berglund, H., Korall, P., Hammarstrom, L., Akermark, B., Styring, S. and Sun, L. C. 1997, J. Am. Chem. Soc., 119, 10720.
84. Hoffman, M. Z. 1988, J. Phys. Chem., 92, 3458.
85. Sutin, N. and Creutz, C. 1980, Pure Appl. Chem., 52, 2717.
86. Drude, P. and Nernst, W. 1894, Zeit. Phys. Chem., 15, 79.
87. Hepler, L. G. 1957, J. Phys. Chem., 61, 1426.
88. Clark, C. D. and Hoffman, M. Z. 1996, J. Phys. Chem., 100, 7526.
89. Meyer, T. J. 1989, Acc. Chem. Res., 22, 163.
90. Sun, H., Yoshimura, A. and Hoffman, M. Z. 1994, J. Phys. Chem., 98, 5058.
91. Kosower, E. M. and Cotter, J. L. 1964, J. Am. Chem. Soc., 86, 5524.
92. Rillema, D. P., Jones, D. S. and Levy, H. A. 1979, J. Chem. Soc. Chem. Comm., 849.
93. Dokter, A. M. 2003, Water in Confinement: Ultrafast Dynamics of Water in Reverse Micelles., thesis, In Institute for Atomic and Molecular Physics, University of Amsterdam
94. Levinger, N. E. and Swafford, L. A. 2009, Annu. Rev. Phys. Chem., 60, 385.
95. Zinsli, P. E. 1979, J. Phys. Chem., 83, 3223.
96. Dokter, A. M., Woutersen, S. and Bakker, H. J. 2006, P. Natl. Acad. Sci., 103, 15355.
97. Dokter, A. M., Woutersen, S. and Bakker, H. J. 2005, Phys. Rev. Lett., 94, 178301.
98. Faeder, J., Albert, M. V. and Ladanyi, B. M. 2003, Langmuir, 19, 2514.
99. Faeder, J. and Ladanyi, B. M. 2000, J. Phys. Chem. B., 104, 1033.
100. Borsarelli, C. D. and Braslavsky, S. E. 1997, J. Phys. Chem. B., 101, 6036.
101. Borsarelli, C. D. 2005, J. Phys. IV., 125, 15.
102. Borsarelli, C. D. and Braslavsky, S. E. 1998, J. Phys. Chem. B., 102, 6231.
103. Garcia Posse, M. E., Vergara, M. M., Fagalde, F., Mellace, M. G. and Katz, N. E. 2004, J. Argentine Chem. Soc., 92, 101.
104. Webb, T. J. 1926, J. Am. Chem. Soc., 48, 2589.
105. Valero, M., Sanchez, F., Gomez-Herrera, C. and Lopez-Cornejo, P. 2008, Chem. Phys., 345, 65.